

Magnesium Ferrite Sensor for H₂S Detection

Takeshi Hashishin,* Hiroyuki Onoda,¹ Tomoe Sanada,¹
Daiki Fujioka,¹ Kazuo Kojima,¹ and Takashi Naka²

Division of Material Science, Functional Material Engineering, Kumamoto University,
2-39-1, Kurokami, Chuo-ku, Kumamoto 860-8555, Japan

¹Department of Applied Chemistry, College of Life Sciences, Ritsumeikan University,
1-1-1 Nojihigashi, Kusatsu, Shiga 525-0058, Japan

²National Institute for Materials Science, 1-2-1 Sengen, Tsukuba, Ibaraki 305-0047, Japan

(Received June 28, 2016; accepted October 11, 2016)

Keywords: MgO, MgFe₂O₄, p–n junction, H₂S

The composite effects of p-type MgO and n-type MgFe₂O₄ on H₂S detection were investigated. The mixture state of these oxides was fixed under coprecipitation conditions: mixture ratio of iron source to magnesium source, and pH control of precursor solution by dropping of an alkaline solution. The composite mixture of MgO, Fe₂O₃, and MgFe₂O₄ was obtained by adjusting the mixture ratio of Fe to Mg. The resistance in air monotonically increased with increasing MgO content in the matrix of MgFe₂O₄. In contrast, the resistance in air decreased with increasing Fe₂O₃ content. The sensing properties of these composites to 3 ppm H₂S were evaluated as a sensor response (*S*), defined as the ratio of the resistance in air (*R*_a) to that in the gas mixture of H₂S and air (*R*_g). The sensor response depended on the composite state of MgFe₂O₄ and MgO because the amount of H₂S adsorbed on the composite was increased by the formation of the p–n junction. In contrast, the sensor response was not improved in the presence of excess MgO in the matrix of MgFe₂O₄, suggesting that the excess MgO serves as an insulator in the electron transfer between the semiconductor composite MgO–MgFe₂O₄ and an interdigitated Pt microelectrode.

1. Introduction

Semiconductor metal oxide (SMO) gas sensors have become one of the major tools in gas detection. Among SMOs, n-type SnO₂,^(1–4) ZnO,^(5–8) TiO₂,^(9–11) and WO₃^(12,13) are widely used as gas sensors. The sensing properties of a solid solution sensor with a spinel structure, i.e., MFe₂O₄ (*M* = divalent metal), have been evaluated using CO, CO₂, CH₄, C₂H₅OH, H₂S, C₂H₅COOH, O₂, H₂, Cl₂, NH₃, CH₃COOH, gasoline, acetylene, and liquid petroleum gas (LPG).⁽¹⁴⁾ In the case of *M* = Ni, nickel ferrite was used for the first time as a sensor to detect a low concentration of chlorine gas.⁽¹⁵⁾ In this study, the detection limit was 2 ppm. Besides, nanocrystalline NiFeMnO₄ thick films indicated high selectivity at 350 °C to 1000 ppm H₂S, i.e., 4-fold higher than that to LPG, CO₂, C₂H₅OH, NH₃, and Cl₂.⁽¹⁶⁾ This selectivity was based on the fact that H₂S is oxidized by the adsorbed oxygen (O[−]) generated at more than 350 °C. The ferrite compounds MFe₂O₄ (*M* = Cu, Zn, Cd, and Mg) have been developed for the detection of acetylene, CO, LPG, H₂, and C₂H₅OH in the concentration range of 1000 to 6000 ppm.⁽¹⁷⁾ The hole concentration was decreased by the reaction

*Corresponding author: e-mail: hashishin@msre.kumamoto-u.ac.jp

of alcohol with ZnO/ZnFe₂O₄ film such as methanol, ethanol, and propanol. The doubly charged oxygen vacancy formed during the reaction was eliminated by the hole of the ZnO/ZnFe₂O₄ film.⁽¹⁸⁾ Ferrite compounds have high corrosion resistance⁽¹⁹⁾ and oxidation resistance,⁽²⁰⁾ which are important features of a gas sensor. Thus, ferrite could be an attractive candidate gas sensor with low cost and high stability. The MgFe₂O₄ pellet sensor showed that the sensor responses (ratio of resistance in air to resistance in gas) to petrol gas and hydrogen sulfur were 3.0 and 1.2 at 250 °C, respectively.⁽²¹⁾ The response of the ferrite gas sensor should be improved for domestic and industrial purposes.

In general, p–n junction effects are adopted to enhance the sensor response of an oxide semiconductor.^(22,23) The formation of a p–n junction contributes to the enlargement of the depletion layer on the surface of the oxide semiconductor, leading to the increase in the amount of adsorbed oxygen (O⁻). As a result, the sensor responses to oxidizing or reducing gases increase with the interaction of the adsorbed oxygen with the gases.

Magnesium ferrite is composed of p-type MgO and nonconductor Fe₂O₃. The solid solution of both oxides behaves as an n-type semiconductor. In this study, we focused on the complex effects of p-type MgO and n-type MgFe₂O₄ on H₂S detection. The coprecipitation method was adopted to obtain magnesium ferrite, on which both cations of Mg and Fe were simultaneously deposited as oxides by adjusting the pH of a highly alkaline solution. The effects of the difference in mixture ratio between Fe and Mg on the product phases and composition were investigated. A water suspension of magnesium ferrite was dropped on the interdigitated Pt electrodes to be a sensor element. The sensing properties of a magnesium ferrite gas sensor to 3 ppm H₂S were discussed on the basis of the correlation between the existence ratio of MgFe₂O₄ to MgO and the resistance in air.

2. Materials and Methods

2.1 Preparation of ferrite

As a typical precipitant, 96 g of NaOH was dissolved in 400 mL of H₂O to obtain 6 M NaOH aqueous solution. In this study, iron nitrate and magnesium acetate were used as starting substances on the basis of a report⁽²⁴⁾ indicating that magnesium ferrite could be obtained at low temperatures using an iron nitrate–barium acetate system rather than an iron nitrate–barium nitrate system. The starting materials, i.e., Fe(NO₃)₃·9H₂O and Mg(CH₃COO)₂·4H₂O, were stirred for 1 h in 200 mL of H₂O to obtain a predetermined ratio of Fe to Mg. Continuously, the 6 M NaOH aq. solution was added dropwise in the solution mixture containing Fe and Mg until a pH of 11 was reached. Herein, note that the excessive dropping of the NaOH aq. solution contributed to the increase in sodium ion concentration, leading to sodium contamination. The coprecipitate obtained after stirring and aging for 1 d was washed in water to remove impurity ions. The precipitate was calcined at 800 °C for 3 h to promote crystallization.

2.2 Fabrication of microsensor

2.2.1 Preparation of ferrite suspension

0.5 g of coprecipitate obtained in Sect. 2.1 was dispersed in 20 mL of deionized water. This suspension and 35 g of zirconia balls of 2 mm diameter were placed in a 50 mL ball milling vial, and this vial was rotated for 20 h to obtain a suspension with fine particles.

2.2.2 Dropping ferrite suspension on interdigitated Pt electrodes

Pt was adopted as the component of interdigitated electrodes to avoid peeling metal electrodes off the SiO₂/Si substrate at a high temperature of more than 600 °C. The interdigitated Pt electrodes were fabricated on the SiO₂/Si substrate by ultraviolet photolithography, as seen in Fig. 1(a). 0.2 μL of suspension prepared in Sect. 2.2.1 was dropped five times on the electrodes and dried gradually at 35 °C for half a day to obtain a sensing film. The sensing film was calcined at 800 °C for 3 h to obtain a ferrite microsensor.

2.3 Characterization of ferrite

2.3.1 Identification of product phase

The coprecipitate obtained in Sect. 2.1 dried at 100 °C for 1 d was hand-grounded for 10 min to avoid the aggregation of ferrite grains. The grounded particles were calcined at 800 °C for 3 h and became fine via hand grinding for powder X-ray diffraction. The product phases were identified using an X-ray diffractometer (XRD, Ultima IV, Rigaku, Japan), equipped with a Ni-filtered Cu K α radiation source ($\lambda = 0.154178$ nm).

2.3.2 Sensing properties of ferrite microsensor to 3 ppm H₂S

The ferrite microsensor was introduced into a flow apparatus equipped with an electric furnace. The sensor resistance (R) of the microsensor was connected to a direct current circuit with power source (E) and standard resistance (r), as shown in Fig. 1(b). The output voltage (V) was corrected at both edges of the standard resistance (r) using a digital multimeter. The sensor resistance (R) was calculated using the equation $R = (E/V - 1)r$. The electrical resistance of the microsensor was measured in air (R_a) and in H₂S-containing air (R_g) at 350 °C. The sensor response was defined as R_g/R_a . The H₂S concentration was precisely fixed to 3 ppm using a mass flow controller (MFC).

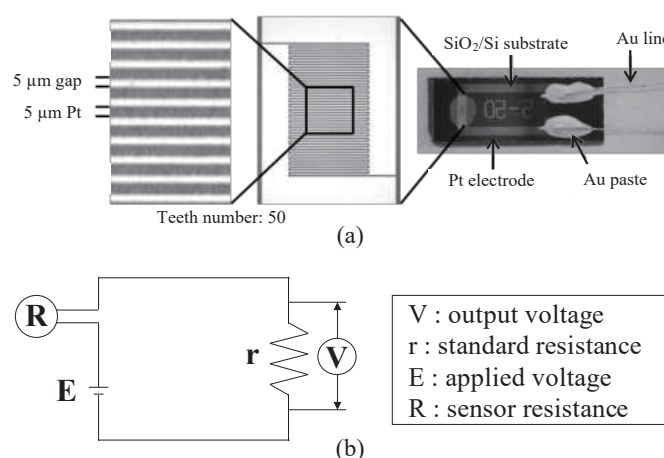


Fig. 1. Schematic drawing of (a) interdigitated Pt electrodes fabricated on SiO₂/Si substrate by UV-photolithography, and (b) electric circuit for gas detection.

3. Results and Discussion

3.1 Effects of Fe and Mg contents on product phase

The XRD patterns of the coprecipitate calcined at 800 °C for 3 h are shown in Fig. 2. The (220) peak of MgFe_2O_4 (ICDD: PDF#01-088-1943), denoted by a square, only appeared at $2\theta = 30.1^\circ$ at all mixing ratios of Fe:Mg. The (104) peaks of Fe_2O_3 (ICDD: PDF#00-033-0664), denoted by circles, independently appeared at $2\theta = 33.2^\circ$ at the mixing ratios of Fe:Mg = 7:3, 6:4, 5:5, and 4:6. The peaks of MgO (ICDD: PDF#01-087-0653) overlapped with those of MgFe_2O_4 . As seen in the upper graph of Fig. 3, the amount of both phases formed was estimated as the relative intensity ratio of MgFe_2O_4 to MgO by summation from the first to third peaks in the diffraction intensity ranges of MgFe_2O_4 and MgO in Fig. 2 because both peaks cannot be separated from each other. Furthermore, the relative peak intensity calculated based on the summation from the first to third peaks of respective Fe_2O_3 , MgFe_2O_4 , and MgO was plotted as a function of Mg content in the lower graph of Fig. 3. The amount of MgFe_2O_4 formed tended to reach its maximum at 40 mol% Mg (Fe:Mg = 6:4) and decrease over 50 mol% Mg, i.e., more than Fe:Mg = 5:5. This tendency is caused by the increase in the MgO content of product phases. In general, it is known that MgO content increases more than Fe:Mg = 5:5 in the binary system of the Fe_2O_3 -MgO phase diagram.⁽²⁵⁾ In contrast, the amount of MgFe_2O_4 formed was decreased to less than 30 mol% Mg, i.e., Fe:Mg = 7:3. The amount of Fe_2O_3 was relatively decreased with increasing Mg content. This tendency corresponded to increasing the MgO content. From the above results, the summation from the first to third peaks in the diffraction intensity ranges of MgFe_2O_4 and MgO and comparison with the relative peak intensity of three oxides are significant in order to estimate the amount of MgFe_2O_4 relative to that of MgO in the MgFe_2O_4 solid solution.

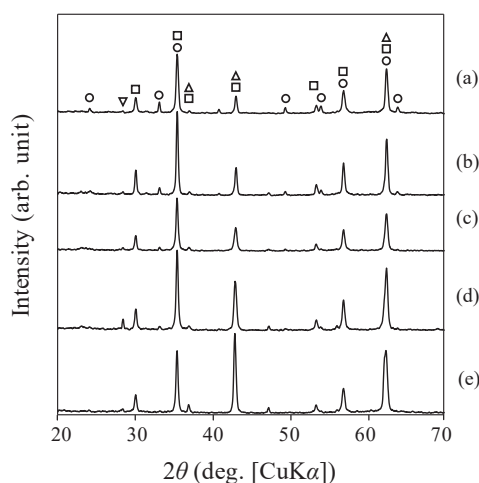


Fig. 2. XRD patterns of product phases calcined at 800 °C for 3 h. The mixing ratios of Fe:Mg are fixed to (a) 7:3, (b) 6:4, (c) 5:5, (d) 4:6, and (e) 3:7 (○: Fe_2O_3 , □: MgFe_2O_4 , △: MgO, ▽: Si).

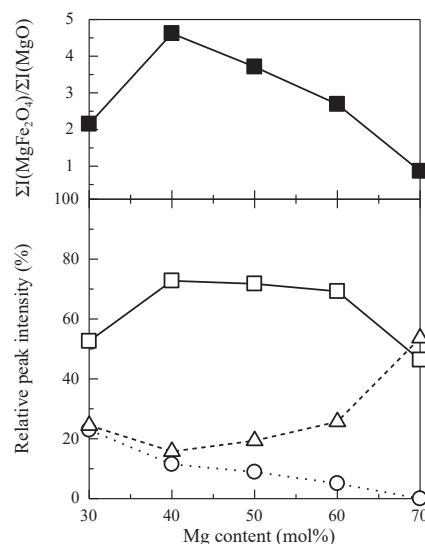


Fig. 3. Relative intensity ratio of MgFe_2O_4 to MgO calculated from the summation from first to third peaks in the diffraction intensity ranges of MgFe_2O_4 and MgO (upper graph) and relative peak intensity of three oxides (○: Fe_2O_3 , □: MgFe_2O_4 , △: MgO) (lower graph).

3.2 Deposition state of ferrite film on microsensor

The surface morphologies of the sensing film obtained at 100 mol% Fe (Fe:Mg = 10:0) were inhomogeneous, and the film was partially peeled off the interdigitated Pt electrodes. In the cases of 90 mol% Fe (Fe:Mg = 9:1) and 80 mol% Fe (Fe:Mg = 8:2), the sensing films had irregular concave and convex surfaces without cracks. The sensing film obtained at 33.3 mol% Fe (Fe:Mg = 1:2) had many large cracks on its surface. The sensing film with peeled parts and large cracks is the cause of the irregularity of the sensing properties to gases. From the above surface morphologies of the sensing films, the film with peeled parts and large cracks was not used for gas detection, whereas the sensing films with smooth surfaces and small cracks could be used for gas detection, as seen in Fig. 4. The sensing films composed of Fe:Mg = 2:1, 7:3, 6:4, 5:5, 4:6, and 3:7 are 4.4, 4.4, 4.6, 3.8, 2.6, and 3.3 μm in thickness, respectively.

3.3 Sensing properties of ferrite microsensor to 3 ppm H₂S

The complex effects of MgFe_2O_4 and MgO are shown in Fig. 5. The R_a of the MgFe_2O_4 and MgO composite monotonically increased with increasing Mg content. The p-n junction between p-type MgO and n-type MgFe_2O_4 contributed to the enlargement of the depletion layer caused by increasing amount of oxygen adsorbate (O^-). In general, the sensor with a higher R_a indicates a higher sensor response without an insulator. The sensor response of the sensing film with 50 mol% Fe (Fe:Mg = 5:5) is maximum, but those with 40 mol% Fe (Fe:Mg = 4:6) and 30 mol% Fe (Fe:Mg = 3:7) tend to be lower, as shown in Fig. 6. On the other hand, the sensing film composed of MgO did not

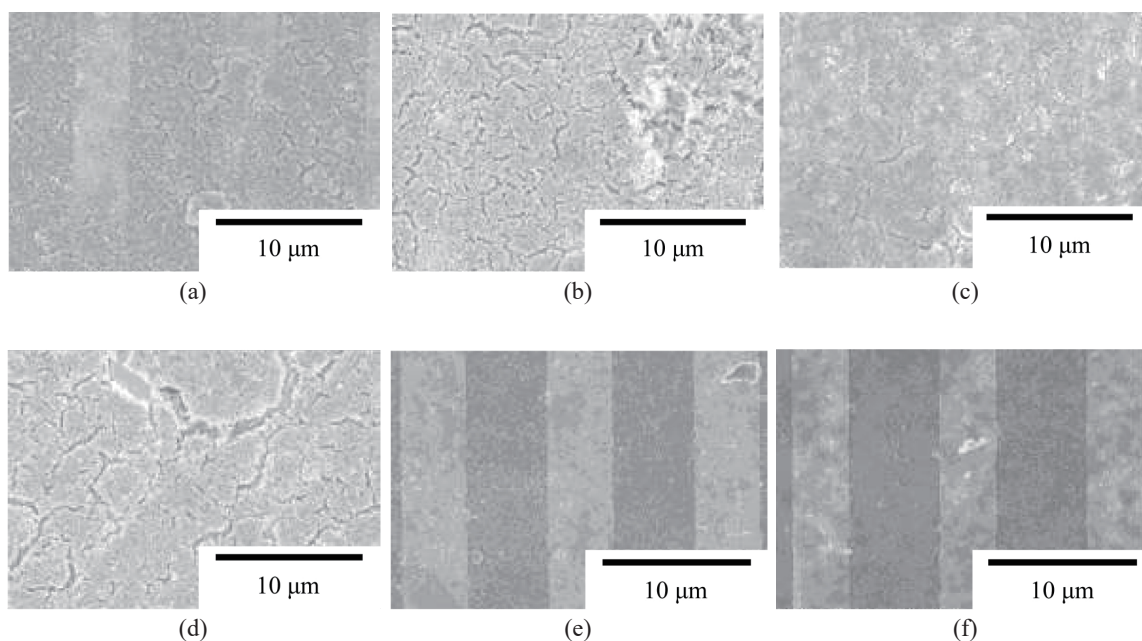


Fig. 4. Surface morphologies of the microsensors calcined at 800 °C for 3 h after dropping a water suspension of magnesium ferrite on interdigitated Pt electrodes. The mixing ratios of Fe:Mg are fixed to (a) 2:1, (b) 7:3, (c) 6:4, (d) 5:5, (e) 4:6, and (f) 3:7.

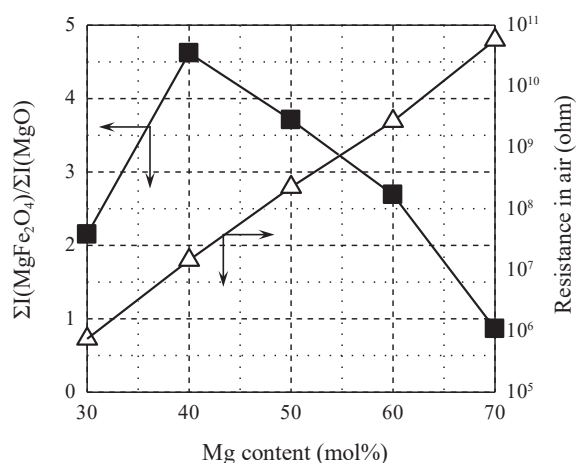


Fig. 5. Relationship between diffraction intensity of $\Sigma I(\text{MgFe}_2\text{O}_4)/\Sigma I(\text{MgO})$ and resistance in air at 350 °C.

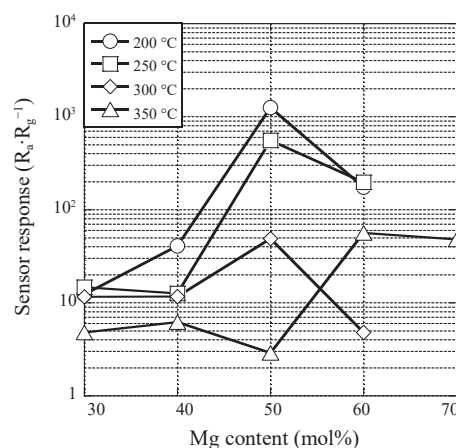


Fig. 6. Sensor response of magnesium ferrite microsensors to 3 ppm H_2S at 200 to 350 °C as a function of Mg content.

indicate sensor response ($S = 1$). Thus, it could be considered that MgO was not related to sensor response, suggesting that the sensing film with more than 50 mol% MgO behaves as an insulator. Even if the adsorption of H_2S is increased by the formation of a p-n junction, the excessive MgO content in the sensing film inhibits electron transfer, leading to a lower sensor response. In the case of the maximum MgFe_2O_4 content in the sensing film (Fe:Mg = 6:4), the sensing film indicated an n-type sensor response. The optimum detection temperature for 3 ppm H_2S was 200 °C in the case of the sensing films with 40 and 50 mol% Mg (Fe:Mg = 6:4, 5:5), caused by the formation of the p-n junction between the p-type MgO and the n-type MgFe_2O_4 . Figure 7 shows representative response-recovery characteristics of the magnesium ferrite microsensors obtained in Fe:Mg = 5:5. The 90% response times at 200, 250, 300, and 350 °C were 18, 84, 96, and 120 s, respectively. The 50% recovery times at 200, 250, 300, and 350 °C were 108, 60, 180, and 243 s, respectively. In Ref. 16, it was described that H_2S was oxidized with the adsorbed oxygen of O^- at the operation temperature from 150 to 450 °C and converted to SO_2 and H_2O as follows: $\text{H}_2\text{S} + 3\text{O}^- \rightarrow \text{SO}_2 + \text{H}_2\text{O} + 3\text{e}^-$. At higher temperature (more than 250 °C), H_2S could be oxidized before reaching the surface of the sensor element, leading to a decrease in the sensor response. The differences of 50% recovery times between 200 and 250 °C might be related to the reaction equilibrium of H_2S and adsorbed oxygen. The dependence of crystallite size of three oxides on Mg content is shown in Fig. 8. The crystallite size was calculated for the maximum peaks of $\text{Fe}_2\text{O}_3(104)$, $\text{MgFe}_2\text{O}_4(311)$, and $\text{MgO}(200)$. The peak of $\text{Fe}_2\text{O}_3(104)$ disappeared at the Mg content of more than 50 mol%. The crystallite size of $\text{Fe}_2\text{O}_3(104)$ ranged from 60 to 120 nm, which was increased with increasing Mg content. The change in crystallite size of $\text{MgFe}_2\text{O}_4(311)$ with increasing Mg content was similar to that of $\text{MgO}(200)$, which was ranging from 20 to 60 nm. From the above results, the roles of three oxides on the sensor response of the magnesium ferrite microsensors could be proposed as shown in Fig. 9. On the basis of the discussion on Fig. 3, it is considered that Fe_2O_3 and MgFe_2O_4 particles act as n-type conductive pass and MgO particles block electric transfer. In Fe:Mg = 7:3 and 6:4,

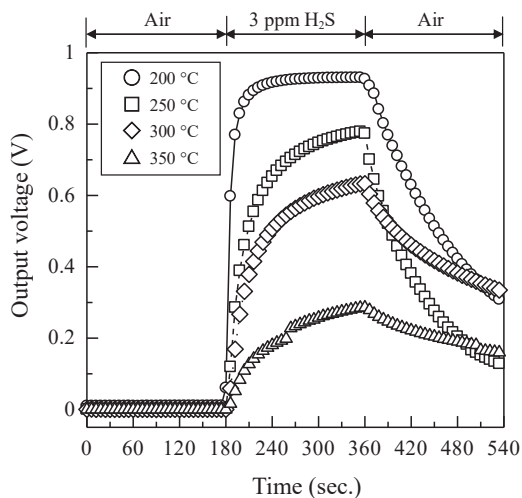


Fig. 7. Response-recovery transients of magnesium ferrite microsensor obtained in Fe:Mg = 5:5, to 3 ppm H₂S at 200 to 350 °C.

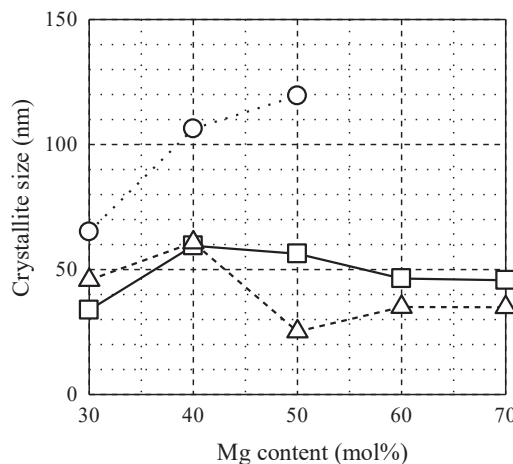


Fig. 8. Crystallite size of three oxides contained in the magnesium ferrite obtained after calcination at 800 °C for 3 h, as a function of Mg content (○: Fe₂O₃, □: MgFe₂O₄, Δ: MgO).

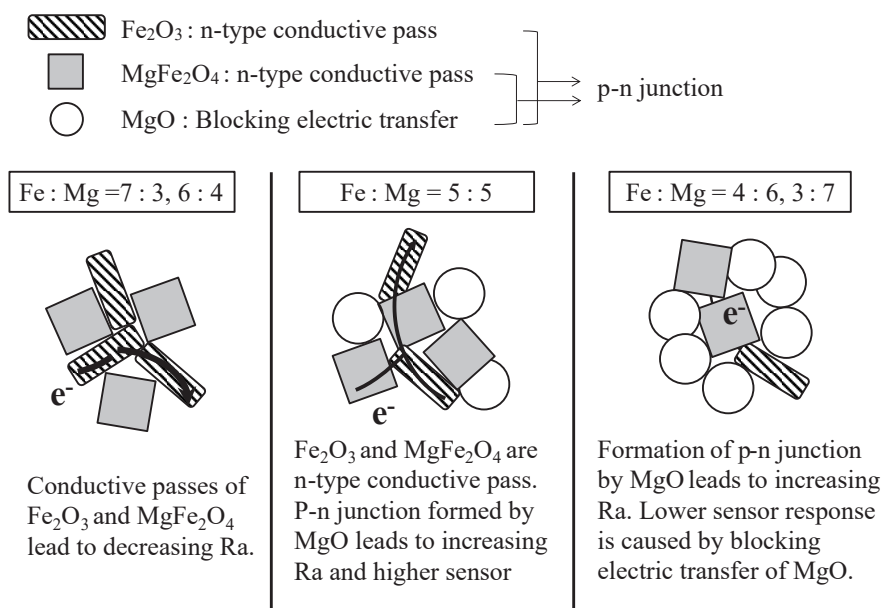


Fig. 9. Role of three oxides on sensor response of magnesium ferrite microsensor.

two oxides of Fe₂O₃ and MgFe₂O₄ lead to decreasing R_a. In Fe:Mg = 5:5, two oxides of Fe₂O₃ and MgFe₂O₄ are n-type conductors, and the p-n junction is formed at the interface between MgFe₂O₄ and MgO. As a result, remarkable improvement appears as the increase in R_a and sensor response. In Fe:Mg = 4:6 and 3:7, a large amount of MgO blocks the electric transfer of the n-type conductive pass of Fe₂O₃ and MgFe₂O₄ as well as forms a p-n junction between MgFe₂O₄ and MgO, leading to an increase in R_a and a decrease in sensor response.

4. Conclusions

The optimum processes in the fabrication of a ferrite microsensor for H₂S detection are concluded as follows: A complex oxide of MgFe₂O₄ and MgO was coprecipitated at the mixing ratios of Fe:Mg = 5:5 and 6:4. The coprecipitate after calcination at 800 °C for 3 h was hand-grounded for 10 min. 0.2 μL of the water suspension was added dropwise five times on the interdigitated Pt electrodes and dried gradually at 35 °C for half a day to avoid peeling and cracks on the surface.

The higher sensor response to H₂S was realized as follows: the sensing films with 40 and 50 mol% Mg (Fe:Mg = 6:4, 5:5) contributed to the formation of the p–n junction between the p-type MgO and the n-type MgFe₂O₄; the optimum detection temperature for 3 ppm H₂S was shifted to a lower value of 200 °C by the p–n junction effect.

Acknowledgements

This work was partially supported by a Grant-in-Aid for Scientific Research, KAKENHI, 395 (25246013).

References

- 1 J. W. Gong and Q. F. Chen: *Sens. Mater.* **18** (2006) 183.
- 2 J. C. Chiou, S. W. Tsai, Y. S. Liu, and C. T. Huang: *Sens. Mater.* **20** (2008) 425.
- 3 Z. Zhang, K. Huang, F. Yuan, and C. Xie: *Sens. Mater.* **26** (2014) 649.
- 4 N. K. Park, T. H. Lee, M. J. Kim, and T. J. Lee: *Sens. Mater.* **27** (2015) 61.
- 5 T. H. Kwon, J. Y. Ryu, W. C. Choi, S. W. Kim, S. H. Park, H. H. Choi, and M. K. Lee: *Sens. Mater.* **11** (1999) 257.
- 6 B. C. Yadav, R. Srivastava, and A. Yadav: *Sens. Mater.* **21** (2009) 87.
- 7 C. C. Hsiao, Y. C. Hu, and R. C. Chang: *Sens. Mater.* **22** (2010) 417.
- 8 Q. Tan, C. Li, W. Liu, C. Xue, W. Zhang, J. Liu, X. Ji, and J. Xiong: *Sens. Mater.* **26** (2014) 447.
- 9 B. R. Deh Kordi, L. Rezazadeh, and P. Keyvanfar: *Sens. Mater.* **16** (2004) 309.
- 10 T. Arakawa, H. Yasukawa, and K. Fujimoto: *Sens. Mater.* **22** (2010) 201.
- 11 Z. Meng, A. Fujii, T. Hashishin, N. Wada, T. Sanada, J. Tamaki, K. Kojima, H. Haneoka, and T. Suzuki: *J. Mater. Chem. C* **3** (2015) 1134.
- 12 Z. Meng, C. Kitagawa, A. Takahashi, Y. Okochi, and J. Tamaki: *Sens. Mater.* **21** (2009) 259.
- 13 T. Itoh, I. Matsubara, J. Tamaki, K. Kanematsu, W. Shin, N. Izu, and M. Nishibori: *Sens. Mater.* **24** (2012) 13.
- 14 A. B. Gadkari, T. J. Shinde, and P. N. Vasambekar: *IEEE Sens. J.* **11** (2011) 849.
- 15 C. V. Gopal Reddy, S. V. Manorama, and V. J. Rao: *Sens. Actuators, B* **55** (1999) 90.
- 16 R. S. Pandav, A. S. Tapase, P. P. Hankare, G. B. Shelke, and D. R. Patil: *IJRITCC* **3** (2015) 5152.
- 17 N. S. Chen, X. J. Yang, E. S. Liu, and J. L. Huang: *Sens. Actuators, B* **66** (2000) 178.
- 18 K. Arshak and I. Gaidan: *Mater. Sci. Eng. B* **118** (2005) 44.
- 17 N. S. Chen, X. J. Yang, E. S. Liu, and J. L. Huang: *Sens. Actuators, B* **66** (2000) 178.
- 18 K. Arshak and I. Gaidan: *Mater. Sci. Eng. B* **118** (2005) 44.
- 19 J. M. A. Van Der Horst: *Metallography* **3** (1970) 433.
- 20 G. Q. Chen, N. N. Li, X. S. Fu, and W. L. Zhou: *Powder Technol.* **230** (2012) 134.
- 21 P. P. Hankare, S. D. Jadhav, U. B. Sankpal, R. P. Patil, R. Sasikala, and I. S. Mulla: *J. Alloys Compd.* **488** (2009) 270.
- 22 J. Tamaki, T. Maekawa, N. Miura, and N. Yamazoe: *Sens. Actuators, B* **9** (1992) 197.
- 23 T. Hashishin and J. Tamaki: *Sens. Mater.* **21** (2009) 265.
- 24 H. I. Hsiang and R. Q. Yao: *Mater. Chem. Phys.* **104** (2007) 1.
- 25 V. Raghavan: *J. Phase Equilib. Diffus.* **31** (2010) 368.